Probability and consequence of post-fire erosion for treatability of water in an unfiltered supply system

Petter Nyman[1,2], Peter Yeates[3], Christoph Langhans[1,4], Philip J Noske[1], Nadav Peleg[5], Christine Schärer[5], Patrick NJ Lane[1], Shane Haydon[6], Gary J Sheridan[1]

[1]University of Melbourne, Baldwin Spencer Building, Parkville, VIC 3010, Australia

[2]Alluvium Consulting, 105-115 Dover Street Cremorne, VIC 3121, Australia

[2]Hydronumerics Pty Ltd, 03/757 Bourke St, Docklands, VIC 3008, Australia

[3]Netherlands Environmental Assessment Agency (PBL), The Hague, 2594 AV, The Netherlands

[4]ETH Zurich, Stefano-Franscini-Platz 5, 8093 Zurich, Switzerland

[5]Melbourne Water Corporation, 990 La Trobe Street Melbourne, VIC 3001, Australia

Corresponding author: Petter Nyman (nymanp@unimelb.edu.au)

Key Points:

- Consequence of wildfire for an unfiltered water supply system is modeled based on erosion, stochastic rainfall and reservoir hydrodynamics
- There is a 10-30% chance that water is untreatable for >1 year due to high suspended sediment concentration after a high severity wildfire
- Assumptions about spatiotemporal rainfall patterns, reservoir hydrodynamics, and erosion are all important sources of error in risk

Abstract

Forested catchments are critical to water supply in major cities. Many of these catchments face the threat of post-wildfire erosion, which can contaminate reservoir water. The aim of this paper is to determine the probability and duration of disruptions to treatability due to runoff-generated debris flows in the first year after a wildfire, before substantial vegetation recovery takes place. We combine models of reservoir hydrodynamics, post-fire erosion, and a stochastic rainfall to determine probability and magnitude of sediment concentration at the reservoir water offtake. Central to the paper is our technique for linking model components into a risk framework that gives probabilities to the number of days that the turbidity threshold for treatment is exceeded. The model is applied to the Upper Yarra reservoir, which is the linchpin the water supply system for Melbourne in SE Australia. However, the framework is applicable to other unfiltered water supply systems where suspended sediment are a risk to treatability. Results show that post-wildfire erosion poses a substantial threat, with a relatively high probability (annual exceedance probability = 0.1- 0.3) of water being untreatable for > 1 year following a high-severity wildfire. Important factors that influence the risk include post-wildfire runoff potential, reservoir temperature and the amount of clay-sized grains in eroding headwaters. Assumptions about spatial-temporal rainfall attributes, reservoir hydrodynamics, and the catchment erosion potential are all important sources of error in our estimate of risk. Our approach to risk quantification will help support planning, risk management and strategic investment to mitigate impacts.

Keywords: wildfire, treatability, water supply, debris flow, reservoir hydrodynamics

1. Introduction

Large cities around the world source their drinking water from forested catchments, which deliver water that is treatable at minimal cost. These forests are often prone to wildfire, which tend to increase surface runoff, destabilize soils and trigger increased sediment delivery into water reservoirs [*Emelko et al.*, 2011; *Hohner et al.*, 2019; *Sheila F. Murphy et al.*, 2015; *Rhoades et al.*, 2011; *Smith et al.*, 2011]. The consequences of wildfire for water supply are a significant concern, with the potential for extended periods of water supply disruption, increased water treatment cost. There is a demand for models to inform catchment restoration, fuel management, and investment in treatment infrastructure [*Bladon et al.*, 2014; *Hohner et al.*, 2016; *Jones et al.*, 2017; *Smith et al.*, 2011; *White et al.*, 2006; *Writer et al.*, 2014].

With increased data availability and improved models, the impacts of wildfire on erosion and sediment delivery from hillslopes and catchments can be predicted with some confidence, or at the least with a specified measure of uncertainty [*Langhans et al.*, 2016; *McGuire et al.*, 2016; *Robichaud et al.*, 2016; *Vieira et al.*, 2014]. Some of these models can be used to assess threats to water resources, currently and into the future with different management strategies [e.g. *Gould et al.*, 2016; *Jones et al.*, 2017; *Sankey et al.*, 2017]. While, generally, there are sophisticated modelling frameworks linking climate, hydrology and water supply management that account for turbidity [e.g. *Porter et al*., 2015], there are few attempts at translating models of post-fire catchment processes to impacts on treatability of reservoir water. Post-fire erosion models are therefore underutilized when it comes to informing reservoir managers about risk.

Metrics of risk provide a quantitative means for cost-effective and evidence-based mitigation [*Khan et al.*, 2015; *Nyman et al.*, 2013; *Thompson and Calkin*, 2011]. In the context of wildfire and treatability of source water, we here define risk as the probability, severity and duration of contamination events at the reservoir offtake, where water is extracted for treatment. With this definition of risk, the consequence of post-wildfire erosion for water supply is a function of i) frequency and magnitude of erosion in headwaters, ii) the transport processes of sediment to the reservoir, and iii) ultimately the propagation of pollutant plume from input location to water offtake. Developing a predictive model of these processes is a large undertaking in terms of data needed for parametrizing and testing models of catchment erosion and reservoir hydrodynamics. However, connecting erosion processes in catchments with sediment transport in reservoirs is paramount to planning and preparedness, and it is needed to provide water supply managers with suitable metrics to evaluate cost and benefits of different options for mitigation and adaptation [*Khan et al.*, 2017]. Options include investment in fuel reduction, active fire-management (suppression), filtration capacity, diversifying water sourcing options, and prevention of particulates reaching the reservoir [*Khan et al.*, 2015; *Thompson and Calkin*, 2011].

In this study, we are motivated by the need amongst water supply managers to know *'For how long is it likely that my reservoir will be offline due to contamination by post-wildfire erosion?* The aims of this research are therefore to:

1. Develop a model to quantify the probability and duration of disruption to treatability due to debris flows in the first year after wildfire, before substantial vegetation recovery takes place.
2. Apply the model to the Upper Yarra catchment, which forms the linchpin of the water supply system for the city of Melbourne in SE Australia.

3. Evaluate the model results in terms of risk to Melbourne's water supply, the sources of error in model estimates, and the implications of our results for mitigation.

Central to our modelling approach is the coupling of reservoir hydrodynamics, post-fire erosion potential, and stochastic rainfall to estimate duration and probability that turbidity thresholds for treatability are exceeded at the reservoir offtake. Note that in this study we only consider sediment in our risk model. Unlike most water supplies for developed countries, the majority of the water supply for the city of Melbourne is from forested catchments, and while it is disinfected, it is unfiltered, therefore relatively small changes in color and turbidity may have a significant impact on drinking water quality. These impacts can be on aesthetics, but more importantly, can impact disinfection efficacy. Impacts on water supply due to elevated dissolved organic carbon, reduced flocculation, and toxic disinfection byproduct [e.g. *Hohner et al.*, 2019; *Stone et al.*, 2011; *Writer et al.*, 2014] are not considered in this study. However, the framework presented is useful in developing risk metrics that comprise these other sources of contamination, which are linked to hillslope processes and reservoir hydrodynamics [*Murphy et al.*, 2015; *Writer et al.*, 2014].

2. Model framework

The model is an implementation of the conceptual framework by *Nunes et al.*, [2018] for assessing water contamination risk. It includes three major components for predicting the probability and duration of treatability disruptions:

1. Propagation of fine sediment within the reservoir, from entry points to the offtake.
2. Susceptibility of the landscape to extreme erosion events.
3. Stochastic spatial-temporal rain fields which cause erosion.

The models are coupled conceptually in a risk framework for predicting the probability and duration of water contamination events that exceed treatability thresholds (Figure 1).

<<<<<<<<<<<<<<Figure 1 here>>>>>>>>>>>>>>>>

In presenting the model and the results in Section 3 and 4 we begin with the processes that govern the transport of sediment between the reservoir boundary and the water offtake at the dam. With this we produce a reservoir transfer function, which is an empirical relation for linking magnitude of sediment delivery events at the reservoir boundary to sediment concentration at the water offtake (Figure 1). As sediment delivery and reservoir transfer functions were calculated independently, no spatially direct coupling of the two components was computationally feasible for each possible event. Instead, the link was realized by choosing four inflow locations that represent expected inflow from post-fire sediment delivery events (Figure 2). Three of the four points represent inflow through the three main tributaries, while the fourth point represents a typical location for inflow from first- or second- order catchments adjacent to the reservoir, about halfway between the reservoir offtake and the main tributaries. After describing the reservoir model, we present the catchment erosion response model, which predicts rainfall thresholds for debris flows in contributing headwater catchments that are all simulated as being burned, but at variable fire severities. Finally, we simulate the actual sediment delivery from headwaters to the reservoir boundary, using rainstorms from two types of stochastic rainfall generators.

In our risk model, we assume most of the water contamination risk is associated from post-fire erosion can be attributed to debris flows. Debris flows produce sediment loads that are ~2 orders of magnitude higher than erosion by other processes [*Noske et al.*, 2016] and have been linked to nearly all major water quality concerns in the Victorian uplands (SE Australia) following several large wildfire that have occurred in 2003, 2007, 2015 and 2009 [*Lyon and O'Connor*, 2008; *Nyman et al.*, 2011; *Smith et al.*, 2011; *White et al.*, 2006]. Once delivered to the stream network, the fine-grained material produced by debris flows is efficiently transported in suspension to downstream assets [*Lyon and O'Connor*, 2008; *Nyman et al.*, 2020]. In their sediment budget for a post-fire debris flow in a geomorphic setting (steep dissected uplands with confined valleys) similar to the Melbourne's water supply catchments, *Nyman et al.* [2020] found that for silt and clay-sized grains, only ~10% of eroded sediments were deposited in the drainage networks linking debris-flow producing headwaters and streams. The justification for developing the model around debris flow as the dominant process for assessing water quality risk in Melbourne's water supply catchment is described in *Langhans et al.* [2016], where the catchment response model was developed.

3 Methods

3.1. Study area

The model was applied to the Upper Yarra (UY) catchment (~337 km^2), comprising mainly sedimentary rocks, and located in the southern region of the Eastern Uplands geomorphic region of Victoria in SE Australia (Figure 2). The climate is temperate with warm, dry summers and cool, wet winters. With strong rainfall seasonality and eucalyptus-dominated vegetation, the region supports some of the most productive and flammable forest ecosystems on earth [*Bowman et al.*, 2009]. The UY catchment is completely covered by forests. However, with a relief of 870 m (elevation range: 321-1191 m.a.s.l.) there are large differences in rainfall and vegetation from low to high elevations. Typically, at lower elevations the vegetation consists of open and dry mixed-species *Eucalyptus* forests. At higher elevations, or on polar-facing (mesic) slopes, the catchment consists of tall and damp or wet *Eucalyptus* forests, often dominated by Mountain Ash (*Eucalyptus regnans*). Annual rainfall ranges from 1200 mm yr^{-1} in at the lower elevation, to 1800 mm yr^{-1} at the catchment divide. The geology is predominantly sedimentary, with clay loam soils. The data used in the development of the erosion response models are sourced from sedimentary lithologies with hydrological attributes and landforms similar to those in the Upper Yarra catchment. In implementing the risk model in the Upper Yarra catchment, we assume that the similarities in geologic and hydroclimatic settings means that our model of erosion response after wildfire is transferrable from one catchment to another. This assumption is supported by our model validation (Figures S4 and S5 in Supporting Information)

<<<<<<<<<<<<<<Figure 2 here>>>>>>>>>>>>>>

The UY catchment drains into a 200 GL reservoir that is central to the potable water supply of Melbourne, SE Australia, a city of more than 4 million people. The reservoir was created in 1957 when a 90 m dam structure was completed to impound the Yarra River. The catchment of the UY dam is a National Park whose primary purpose is for water supply. Access to the catchment is restricted, there is no habitation, forestry, mining, agriculture or recreational activities. The UY reservoir receives transfers from the larger nearby Thomson Reservoir. Together, the Thomson and UY reservoir make up the Silvan system, which provides ~ 60% of Melbourne’s water supply. In the Silvan system, unfiltered water from the UY reservoir is transferred to smaller off-steam storages before disinfection (by chlorination and UV irradiation) and supply into the metropolitan distribution network. The UY reservoir does not have a filtration treatment plant and the water supply goes offline when turbidity exceeds 5 NTU (Nephelometric Turbidity Units). In the event of UY going offline, there would be major disruptions to water supply in the form of water restrictions, boiling water notice, and large costs of sourcing alternative supplies (e.g. desalination water). The hydrodynamics of the UY reservoir are dominated by strong summer thermal stratification and deep winter mixing

3.2. Reservoir hydrodynamics model

The propagation of the sediment plume from input location to dam offtake was modelled using the three-dimensional Aquatic Ecosystem Model (AEM3D), which is an updated version of the Estuary and Lake COmputer Model (ELCOM). The model solves the unsteady Reynolds-averaged Navier-Stokes equations and scalar transport equations with the Boussinesq approximation and hydrostatic pressure terms using the numerical methods described by *Casulli and Cheng*, [1992] and *Hodges et al.*, [2000]. Previous applications of ELCOM are widely referenced in limnological studies [*Trolle et al.*, 2012], including studies of reservoir hydrodynamics and sediment transport [*Dissanayake et al.*, 2019; *Trolle et al.*, 2012]. AEM3D features in more recent publications describing reservoir and lake modelling [e.g. *Madani et al.*, 2020*; Ryu et al.*, 2020; *Tranmer et al.*, 2018*; Valipour et al.*, 2019*; Valerio et al.*, 2019*; Zamani and Koch*, 2020]. *Zamani and Koch*, [2020] demonstrate the appropriateness of AEM3D for modelling reservoirs, such as Upper Yarra Reservoir, that have complex bathymetry, steep walls and a wind-mixed surface layer. *Ryu et al.*, [*2020*] use measurements of water level, flow velocity, temperature and conductivity to demonstrate the ability of the model to predict mixing of density flows in a reservoir.

Sediment concentrations in AEM3D are prescribed in the inflow boundary conditions and calculated in each model cell after accounting for transport, vertical mixing, settling and resuspension. Concentrations are tracked in groups (e.g. fine clay, clay, silt, fine sand, etc) of equal diameter and density and are aggregated to determine total sediment concentrations.

Sediment transport is modelled using the mass-conservative ULTIMATE-QUICKEST scalar transport solver [*Leonard*, 1991] based on the velocity field derived by the hydrodynamics solver. Vertical mixing is modelled using a 3D mixed-layer energy budget approach that includes terms for convective mixing, wind mixing and internal and boundary shear [*Hodges et al.*, 2000. Flocculation was not considered in this study, so the diameter and density of the inflowing sediments do not change in the reservoir. It has been assumed that any contribution from resuspension is negligible, which is a reasonable assumption given that Upper Yarra is a deep reservoir with low bottom shear stress. Sediment density and concentration contribute to water density so that high inflow sediment concentrations increase the plunging depth of inflow intrusions.

AEM3D (and previously ELCOM) models have been developed for Melbourne Water's key water supply reservoirs [e.g. *Morillo et al.*, 2006*; Marti et al.*, 2011] as components in an overarching decision support system [*Mills et al.*, 2011]. A model for Upper Yarra Reservoir was first developed in 2006 to assess the dynamics of inflow intrusions and was calibrated and validated using data collected with a combination of thermistor chains and a fine-scale profiler [*Dallimore and Imberger*, 2006]. Further verification of the model performance was undertaken when the first large post-drought inflow into Upper Yarra Reservoir was observed in June 2012 after a storm in the catchment [*Stevens et al., 2012*].

3.3 Post-fire debris flow model

The model of probability and magnitude of sediment delivery from runoff generated debris flows to the reservoir is based on earlier work by *Langhans et al.* [2016] and *Nyman et al.* [2015]. Model structure, calibration and validation are described in the Supporting Information. In summary, debris flow occurrence is determined from a threshold stream power (Ω_{crit}) at the outlet of small zero-order headwater (~2 ha). The stream power, Ω, is a function of discharge and slope and the threshold, Ω_{crit}, varies depending on the mass of non-cohesive surface material (m_{nc}) that is available on the hillslopes. If m_{nc} is high, the Ω required to incise the channel and trigger a debris flow is lower than if the mass is low. This concept is based on the assumption that the initiation of runoff-generated debris flows is caused by combined shear stresses of water flow and granular fronts formed by hillslope debris flows [*Langhans et al.*, 2017]. The production of surface runoff is modelled with the kinematic wave equation in KINEROS2 [*Woolhiser et al.*, 1990] and controlled by soil hydraulic parameters that vary as functions of fire severity (change in normalized burn ratio, dNBR) and aridity index (AI), both of which are related to the soil hydraulic properties that control infiltration [*Moody et al.*, 2015; *Van der Sant et al.*, 2018]. The magnitude of erosion by debris flows were estimated based on empirical relations in *Nyman et al.*, [2015], whereby erosion on hillslopes and in channels is a function of a stream power index (product of local slope, S (m m^{-1}), and contributing area, A (m^2) (Equations (4-8) and Figure S1 in Supporting Information).

3.4 Model implementation in the Upper Yarra Reservoir

3.4.1 Reservoir hydrodynamics: transfer function and model sensitivity

The propagation of sediment plumes in the UY reservoir were simulated in AEM3D using a range of potential debris flow scenarios. Scenarios varied in terms of debris flow sediment delivery location (one of four different locations shown in Figure 2b) and sediment load. The objective was to model the propagation of the resultant sediment plumes and output a timeseries of predicted sediment concentration at the offtake for each scenario. A suitable range of sediment loads was determined by considering 5 levels of erosion response, ranging from the lowest (in the case of a very small area (~30 ha) producing debris flows) to the highest possible (all contributing headwaters producing debris flow). This approach results in transfer functions that relate sediment loads from the catchments to sediment concentration at the water offtake for a wide range of possible debris flow responses that could eventuate after a wildfire. The range of sediment load scenarios are developed based on assumption about the number of debris flow producing catchments and sediment load estimates from the model described in Figure S1 in Supporting Information). The propagation of sediment plumes was simulated for sediment delivery events at 4 input locations (Figure 2b) that represent a range of possible scenarios of debris flow response in headwaters. Discharge during the sediment delivery events was based on the maximum rainfall depth (35 mm) reported by *Nyman et al.* [2015] for post fire debris flows in Victoria, and by assuming that 100% of runoff from the headwater areas generated debris flows. This will overestimate runoff in the debris flow producing headwaters, however this is offset by the underestimation of runoff from adjacent burned but non-debris flow producing areas that are not currently accounted for in this approach. The combination of debris flow loads, and discharge used in the simulations generate total debris flow sediment concentrations of ~570 g L^{-1} and sediment concentrations of clay of ~ 20-40 g L^{-1}. These are reasonable given the known sediment concentrations in streams below debris flows producing headwaters: 36-59 g L^{-1} at Porepunkah [*Leak et al.*, 2003] and 112 -143 g L^{-1} at Snowy Mountains [*Brown*, 1972].

Post-fire sediment loads were divided into 22 classes of grain diameter ranging from 0.001 to 30 mm. The density of the sediment particles was set at 2650 kg m^{-3} for fines (1.5 mm or less) and 2220 kg m^{-3} for coarser grains (> 1.5 mm). Once entering the reservoir in the AEM3D model at the specific boundary location, the concentration of each of the 22 classes was calculated separately in each model grid cell, as a function of the transport into and out of the cell by background flow and settling rate (determined from particle size, density and following Stokes Law settling velocity calculations). Buoyancy effects associated with plume density, determined as a function of inflow temperature and sediment load, are considered by the model and therefore modify the computed flow field.

The grain size distribution of the sediment delivered to the reservoir by erosion events (Figure S2) was calculated based on data collected during surveys of 10 debris flows in eastern uplands of Victoria [*Nyman et al.*, 2015] (locations are shown in Figure 2), at sites with similar lithology to that of the UY catchment. For each sediment input scenario, AEM3D was run with meteorological forcing provided by observations at 2m above the lake surface taken at 9 min intervals using a moored Lake Diagnostic System (LDS) installed in UY reservoir in September 2005. Data measured in 2006 were selected as representing typical summer conditions over a period of reliable and complete measurements. Inflow and outflow rates monitored by the Melbourne Water SCADA system were used for the reservoir water balance. Thermistor chain data from the LDS and boat deployed CTD profiles have been used in previous studies to calibrate the model [*Dallimore and Imerger*, 2006].

For each sediment input scenario, the number of days that sediment concentration exceeded treatability thresholds at the reservoir offtake was recorded, indicating the period of likely disruptions to treatability. Historically, turbidity at the reservoir offtake is usually under 2 NTU and while excursions above this in the short term are tolerable, turbidities over 5 NTU [likely between 5 and 10 mg L^{-1}: *Lane et al.*, 2006] are regarded as unacceptable from both a disinfection and an aesthetic perspective and not recommended by the Australian Drinking Water Guidelines (ADWG 2011). For our modeling, we therefore set the threshold for treatment at the range of 5-10 mg L^{-1}. The duration (in days) that sediment concentration exceeded this threshold range was plotted against the input sediment load for all five scenarios at each input location. An empirical function was fitted to these outputs and used as transfer function that relates erosion responses to days of undeliverable water. The sensitivity of sediment propagation to parameter inputs was examined in relation to the treatability threshold, grain size distribution, seasonality, and temperature.

3.4.2 Debris flow susceptibility for two wildfire scenarios

The debris flow response model provides a look-up table containing critical stream power (Ω_{crit}) values for combinations of dNBR, slope and aridity of zero-order headwater for the first year after the fire. Loads, M_{df} [t], for each location of a potential debris flow, were estimated at the outlet of first-order channels based on erosion in contributing channels and hillslopes. It is assumed that deposition and erosion in the higher order stream network has little impact on the overall clay loads being delivered to the reservoir. This assumption is supported by findings in *Nyman et al.*, [2020], where measurements and modelling show that a large fraction of clay is generated from hillslopes and colluvium in first-order headwaters. However, expanding on the erosion models to provide a more dynamic link between headwaters and reservoir is an important area for further model development. Values of M_{df} were pre-processed and kept in the lookup table alongside variables related to Ω_{crit} for each zero-order headwater. The approach of using a lookup table and pre-processed loads to represent potential debris-flow response allows for efficient calculation of magnitude and frequency using Monte Carlo simulations, that consider random variation in fire severity and rainfall, as described below.

Scenarios of post-fire debris flow were simulated using fire severity distributions from the Kilmore-Murrindindi (KM) fire that burned in catchments adjacent to the UY catchment during the Black Saturday wildfires in February 2009 (Figure 2a). The wildfire provides fire severity distributions for two distinct periods of burning, representing contrasting fire behavior in forests that are typical of the UY catchment. The two distinct periods of burning are associated with different fire weather. During the first 12 hours of burning, the fire weather was extreme; high wind speeds from the northwest, followed by an abrupt weather change with strong and gusty winds from the southwest [*Cruz et al.*, 2012]. Extreme fire behavior, with crown scorch and burning, persisted until about 5 hours after the weather change. After this time, the fire continued to burn for several weeks during cooler and less windy conditions, resulting in comparably low burn severities, mostly in the understory vegetation (Figure 2a). For our simulations, we consider the first and second periods of burning in the KM fire to represent contrasting fire types: one dominated by crown fire and the other dominated by understory fire.

Fire severity distributions for the low- and high- severity (understory *vs* crown fire) scenarios were produced using the difference normalized burn ratio (dNBR; calculated from Landsat) as a severity metric (Figure 3). The mean dNBR was calculated for individual first-order headwaters that correspond with model response units in Hydrofire. For the high and low severity periods of burning, the number of samples in the KM fire were similar (5414 and 4662 headwaters, respectively). The dNBR were analyzed to determine if there were trends with forest type, aridity, elevation and aspect. No trends were detected. Scenarios of low and high burn severities in the UY catchment were therefore simulated by randomly allocating values to headwaters based on the two distributions, corresponding to low and high severity fires. All headwaters in the catchment were assigned a fire severity, assuming in the simulations that the wildfire affects the entire catchment area. Maps of critical 12-minute rainfall intensities (I_{12_crit}) in individual headwaters were produced taking the median dNBR from 10 random samples from the distributions in Figure 3. Maps of the median annual exceedance probability (AEP) was determined from the median I_{12_crit} and design storm parameters from the Bureau of Meteorology, which are available in a grid (~2.5 km resolution), constructed from 3D spline interpolation of point-based rainfall records [*Ball et al.*, 2016].

<<<<<<<<<<<<<<Figure 3 here>>>>>>>>>>>>>>

3.4.3 Stochastic sediment delivery simulations

The probability and magnitude of sediment delivery to the reservoir were simulated with synthetic rainfall produced from two methods: one based on design storms and depth area reduction factor, the other based on a space-time rainfall generator model. Design storms assume a concentric spatial structure whereby rainfall intensities decline around the storm center according to a depth area reduction factor. On the other hand, space-time rainfall generator models produces rain fields that represent complex spatiotemporal rainstorm structures. The rainfall module from the AWE-GEN-2d model [*Peleg et al.*, 2017; 2019], which is based on the STREAP rainfall generator model [*Paschalis et al.*, 2013], was used to stochastically generate the 2-dimensional storms.

Storms were implemented in Monte-Carlo simulations where each iteration represent a unique erosion scenario in terms of how rainfall intensities overlap with the distribution of fire severity. For both methods, we calculated the total mass of clay (M_c) produced by debris flows, which are triggered when simulated I_{12} exceeded debris-flow rainfall intensity thresholds (I_{12_crit}). The mass of clay (M_c) delivered to the reservoir was predicted once per year assuming that the largest rainfall event captures most of the risk. Thus, the potential for contamination risk to be amplified by multiple storms in a year is not considered. This is a limitation. However, debris flows are typically triggered by rainfall events with AEPs ranging from 0.1 to 0.3 [*Nyman et al.,* 2015], and the area of high erosion potential in the UY catchment is small relative to the size of storm cells. The debris flow conditions, which we assume to be the main source of risk, are therefore unlikely to occur multiple times in the same location during the recovery period.

When simulating erosion with design storms, the rainfall events were sampled at a random location each year using the data grid (~ 2.5 x 2.5 km) with design storm statistics from the Bureau of Meteorology (BoM). Each year, a storm was sampled in each grid cell based on the distribution of annual exceedance probabilities (AEPs) at that cell. Once initiated in a grid cell, the rainfall intensities in surrounding cells decline according to an area reduction factor (λ), which was calculated from the spatial distribution of I_{12} in storms events in the radar archive (Figure S6). Design storms were sampled 150 times in each cell. Sampling of storms was repeated 10 times, resampling fire severity on each iteration. The distribution of sediment delivery events for high and low fire severity scenarios was determined in each cell of the AEP grid by plotting the annual loads as a cumulative distribution function (*cdf*) of annual M_c. The distribution of annual exceedance probability (AEP) for M_c was then estimated from 1-*cdf*.

With the rainfall generator, the rainstorms were simulated over the study area at 6-minute timesteps and aggregated into 24-hour peak I_{12}. A total of 6000 storms (I_{12} between 20 and 200 mm h^{-1}) were created over the catchment. The cell with the highest I_{12} was used to determine the annual exceedance probability (AEP) of the storm based on design storm parameters, which are available from BoM. The debris flow response in headwaters was determined from the peak daily I_{12} across the catchment. Thus, each simulated storm has a known AEP and a simulated clay load (M_c). With 6000 simulations, we obtain a distribution of M_c, which we plotted alongside the model results from design storm simulations. Details on the calibration of the rainfall generator model and examples of synthetic storms are shown in Figure S7.

4. Results

4.1 Reservoir hydrodynamics: Transfer functions and sensitivities

The propagation of suspended sediment from input locations to the reservoir offtake was modelled for individual grain size fractions to examine the relative contribution of different source material to overall contamination risk (Figure 4). Temporal signal of suspended sediment concentration at the offtake is largely caused by grains ≤0.001 mm. The temporal evolution of sediment plume, plotted as curtain cells (Figures S8 and S9), show that this is caused by mixing and prolonged suspension of fine grains within the water column. Larger grains settle more quickly on passage through the reservoir (Figure S9), therefore producing higher concentrations that are confined to layers near the bed.

<<<<<<<<<<<<<<<<Figure 4 here>>>>>>>>>>>>>

The relationship between sediment load and concentration at the water offtake was similar for the four sediment input locations (Sites 1-5: Figure 5). A single function was therefore be fitted to the combined data from all sites. A 2-parameter power law was effective at describing the relation between the two variables (R^2 = 0.88; RMSE = 56 days):

$$D_{>th} = 0.51{M_c}^{0.77} - 44 \qquad (1)$$

By solving for days ($D_{>th}$) = 0, this relation indicates that the input of clay (M_c) must be > 320 Mg for there to be an impact on treatability at the water offtake.

<<<<<<<<<<<<<<<Figure 5 here>>>>>>>>>>>>

Simulations show that the transfer functions are sensitive to the season in which the debris flows occur (Table 1). When compared to the summer simulations, the events in autumn, when water temperature are cooler, are likely to cause concentrations that have lower peaks, but persist for longer periods of time, owing to the increased vertical mixing that occurs in cooler months. The days exceeding 5-10 mg L^{-1} are about 30-50 % higher in autumn than in summer (Table 1).

<<<<<<<<<<Table 1 here>>>>>>>>>>>

Results from other sensitivity analyses indicate that the transfer functions are sensitive to the particle size distribution and debris inflow temperature. For a finer grain-size distribution (25% shift in the distribution in Figure S2), the duration that treatment thresholds are exceeded is up to 58% longer because of a larger contribution to the suspended grains. This increase due to changing grain-size distribution was also dependent on input locations. The transfer functions are moderately sensitive to the temperature of the water transporting sediment into the reservoir with lower or higher input temperatures causing more persistent contamination events. Lowering or increasing the temperature of water discharge by 2 °C (below or above the 22 °C reference temperature for summer simulations) results in up to 20% increase in the days that treatment thresholds are exceeded.

4.3 Debris flow thresholds and probabilities

Rainfall thresholds for debris flows in the first year after wildfire vary strongly with fire severity. For high severity fire scenarios, the median critical 12-min rainfall intensities

(I_{12_crit}) is 166 mm h^{-1} with a range from 48 to 500 mm h^{-1} (Figure 6a). For low severity fire the median I_{12_crit} was 278 mm h^{-1} (range 68 to 500 mm h^{-1}). For both severity scenarios, the median annual exceedance probability (AEP) is 0.01, which means that debris flows are unlikely in most headwaters, irrespective of fire severity. However, the number of headwaters with AEP > 0.01 increases markedly with increasing fire severity (7 *vs* 206 cases for low and high severity scenarios). In general, the area with higher AEP corresponds with the area supported by dry forests, which have the lowest values of hydraulic conductivity in the runoff model, and therefore the highest runoff generation potential. Wet and damp forest at high elevation and on polar-facing hillslopes are unlikely to produce debris flows. Headwaters with highest probabilities are concentrated at low elevations in the northern tributary to the reservoir.

<<<<<<<<<<<<<<<<<<Figure 6 here>>>>>>>>>>>>>>>

4.4 Sediment delivery and consequence for treatability

The distributions of clay loads (M_c) from post-fire debris flows were obtained from storms (design and stochastically generated) sampled at random within the catchment. With the modelled response to each of these storms, we plot distributions of annual exceedance probability (AEP) for the input of clay-sized sediments to the UY reservoir for high and low fire severities (Figure 7 a and c, respectively). There is a large range in M_c for any given AEP. At high AEP, M_c varies spatially by 2-3 orders of magnitude. This means that for these storms the catchment response is very sensitive to where the storm is centered in relation to debris flow thresholds, which are heterogenous and clustered (Figure 6 a and c). For design storms the spatial variation in M_c decreases as AEP decreases, because the infrequent and most intense storms result in debris flow thresholds being exceeded uniformly throughout the catchment. For the storms generated by the rainfall generator, the spatial variation remains high for all AEPs. M_c modelled with design storms are larger than what is produced by the rainfall generator, particularly for high intensity rainfall events (low AEP).

<<<<<<<<<<<<<<<<<<Figure 7 here>>>>>>>>>>>>>>>

All rainfall scenarios within each AEP are equally likely. Therefore, in the context of risk to water supply, we consider the distribution of AEP for the maximum impact (show as red and black solid lines in Figure 7) as being the most relevant. As expected from results in Figure 6, the high severity fire results in much higher probabilities of large M_c than low severity fire (Table 2). The likelihood of disruptions to treatability in the UY reservoir is relatively large for a high severity wildfire (Table 2). The AEP for interruptions ($D_{>th}$) of 50, 100 and 300 days, are 0.45, 0.42 and 0.29, respectively, for design storms. For low severity fire the corresponding values are 0.19, 0.15 and 0.06. Hence, the difference in AEP for a given $D_{>th}$ remain similar for the two fire scenarios across this range of $D_{>th}$. In a relative sense the difference increases from a factor of 2.2 for $D_{>th}$ = 1 month to 5 for $D_{>th}$ = 12 months. The pattern for the storms generated by the rainfall generator is similar, although the AEP decreased more rapidly when $D_{>th}$ > 100 days.

<<<<<<<<<<<<<<<<<Table 2>>>>>>>>>>>>>>>>>>

5. Discussion

5.1 A new framework for predicting risk to treatability in unfiltered water supply systems

The paper presents a comprehensive analysis of risk associated with treatability of water after a wildfire. For the first time, we connect the post-fire erosion responses of catchments to the consequence for treatability of water at the reservoir offtake. The framework presented in Figure 1 links two models with a transfer function (Figure 5). One model predicts the erosion response of headwaters and the other predicts how sediment is propagated through the reservoir. The erosion response is simulated using two methods for generating stochastic rainfall. The framework for linking probability of erosion and consequence for water supply is a significant conceptual development in terms of extracting value from erosion models applied to the water resources sector. It is a template approach for future studies that aim to derive metrics from post-fire erosion models that can be used to guide cost-benefit analysis, investment and policy in the management of catchments for potable water supply [*Khan et al.*, 2015]. Moreover, our approach is strongly aligned with the framework advocated by *Nunes et al.* [2018] whereby the model development is guided by 1) identifying contaminant and assets of concern, 2) understanding the dominant processes that govern contaminant mobilization, and 3) mapping the pathways linking contaminants to areas of concern.

The approach to modeling water quality risk involves two major decisions regarding the conceptual representation of risk. First, the models of sediment delivery from the catchment and the propagation of sediment within the reservoir are coupled via empirical transfer functions (Figure 5). Creating transfer functions from an array of hydrodynamic modelling results that capture the expected range of post-fire sediment load and input locations provides a means to incorporate stochasticity in fire and erosion without computational constraints imposed by the hydrodynamic model, which is time consuming to run. For instance, a single iteration of AEM3D takes ~ 22 hours running 15 cores on a 3.10 GHz Xeon Linux computer. Moreover, by decoupling the two models, our approach allows for greater model tractability in terms of sources of error and the major levers on risk.

Second, the erosion model only considers runoff-generated debris flows as a cause of sediment delivery to the reservoir. In modelling erosion as a threshold process, we seek to achieve parsimony with respect to the dominant processes driving water quality risk [adovated by *Nunes et al.*, 2018], thereby eliminating unnecessary complexity and providing stronger alignment between key hydrological drivers and threat [*Nyman et al.*, 2013]. The decision to consider runoff-generated debris-flows only was justified in *Langhans et al.* [2016], and based on evidence from past observation of water quality impacts from forested catchments in the region [*Smith et al.*, 2011]. However, we emphasize that the framework is generally applicable to water supply systems and can be tailored to other hydrogeomorphic settings where erosion processes may be governed by different processes or where the constituents of concern are different. The reservoir model (AEM3D) is suited for modelling range constituents and biogeochemical processes [*Tranmer et al.*, 2018], so impacts of post-fire hydrology on water quality in lakes and reservoir can be evaluated with AEM3D more generally in the context of impacts on both ecosystem and water supply. The reservoir hydrodynamics model can be refined and tested further to include other issues that are important for treatability of water after wildfire: water quality constituents other than suspended sediment, flocculation processes, and longer-term issues such as algae bloom that stem from post-wildfire nutrient enrichments [*Emelko et al.*, 2016; *Hohner et al.*, 2019].

5.2 Magnitude of risk to treatability and sources of error

The study demonstrates that after high severity wildfire there is a relatively high probability ($0.1 < AEP < 0.3$) of major consequences in the UY reservoir whereby water is untreatable for several months to a year. Water quality impacts of such magnitudes have been previously recorded in the SE Australia region after large erosion events [*Ollerenshaw et al.*, 2014; *White et al.*, 2006]. In Lake Bellfield, landslides and debris flows caused 1-2 order of magnitude increases in turbidity for over one year (2 NTU prior to the erosion event, 38-235 NTU in the first year after the debris flows), and resulted in water that was unsuitable for drinking for at least 3 years [*Ollerenshaw et al.*, 2014]. In Canberra, post-fire erosion including runoff-generated debris flows, caused increased turbidity that made the water unfit for distribution for several months [*White et al.*, 2006], ultimately resulting in the investment in a new treatment plant. Thus, our predictions, showing that the likely interruptions last months to a year, are consistent with some of the observed impacts from large erosion events in the region. The observations also provide some justification for the approach whereby the model considers only the large, threshold-driven erosion response in determining the risk to water quality.

We resort to some simplification and assumptions related to the flow delivering sediment to the reservoir boundary and the propagation of sediment within the reservoir itself. Source of error in model prediction can be evaluated separately for the two model components (Table 3). For sediment delivery by debris flows, the data used in the model development can be used to quantify the magnitude of error caused by debris flow thresholds, the predicted sediment loads and the clay content. For the propagation of sediment within the reservoir, the error was quantified with respect to water temperature, seasonality, the transfer function (Eqn. 1), which comprise errors that stem from variable input locations and assumed suspended sediment threshold for treatment. The magnitude of the error terms depends on the magnitude of $D_{>th}$. For $D_{>th}$ = 30 days (1 month), the transfer function (Eqn. 1) is a major source of error, with RMSE (52 days) that is very high (±177%) relative to the predicted duration of treatability disruption. The relative importance of this error term decreases as the magnitude of impact increases; however, it remains the largest source of error in the model. Developing a narrower threshold range for suspended sediment and treatability would greatly reduce the size of this error term. The debris flow rainfall threshold (determined by *b*: described in Supporting Information), the predicted sediment load from first-order headwaters, and seasonality (events in autumn vs summer) are associated with relative errors that are less than ±12%.

<<<<<<<<<Table 3 here>>>>>>>>>>>>

The study indicates that risk to water supply is highly sensitive to assumptions regarding rainstorms, which drive sediment delivery. When using a design storm to drive the erosion response, the model tends to predict higher sediment delivery than when using storms from a 2d stochastic rainfall generator. This effect can stem from the simple approach to scaling of design storms using depth area reduction factor (λ), which assumes rainfall declines monotonically and symmetrically from the storm center (Figure S6). With this approach, the spatial distribution of rainfall intensities is clustered around a single storm cell, and the contiguous area subject to conditions where $I_{15} > I_{12\_crit}$ is likely to be overestimated, particularly during high intensity storms. The discrepancy between the assumed symmetrical distribution of I_{12} around a storm center as opposed to the more complex spatial patterns of rain appears to have a larger effect during rare events (Figure 7). Higher sediment delivery from design storms may also stem from rainfall intensities scaling less strongly with area (i.e. rainfall intensities reduce at a slower rate with increasing area).

The spatiotemporal storms produced with the rainfall generator model are more realistic (examples shown in Figure S7). However, these are also subject to error that stem from model assumption and data used in the calibration. First, the parameters that determine the spatial scaling of rainfall are obtained from radar rain fields, which come with error associated with the calibration of radar reflectivity with measured rainfall. Across the network of rain gauges (n=48) used in calibrating the Melbourne Rainfall Radar the mean RMSE for rainfall intensities > 5 mm h^{-1} is 5.2 mm h^{-1}. This is low relative to the intensities that trigger debris flows (I_{12} > 50 mm h^{-1}) and unlikely to have large impact on the results. Second, in our implementation of the rainfall generator model, we assume for simplicity the coefficient of variation (CV) in rainfall intensity and wat area ratio (WAR) are kept constant (parameters described in Supporting Information). In addition, the rainfall spatial correlation is assumed to be constant; the duration of the available radar data (5 years) was insufficient for extracting parameters that vary with storm intensity.

5.2 Costs and opportunities for mitigation

The potential costs of wildfire related contamination events in forested water supply catchments are substantial. There are a number of factors to consider when assessing impacts on water supply and costs. Management of water offtakes by regulating the depth of water extraction is one strategy that is likely to provide a means for reducing the duration that the UY reservoir is offline. Our risk analyses points to the large importance of expanding on the reservoir hydrodynamics modelling to better understand the capacity to mitigate risks with reservoir operations. The availability of alternate offtakes at different depths and understanding the location and seasonal behavior of the thermocline are important in risk mitigation. Expanding on our hydrodynamic modelling and developing a framework for evaluating how reservoir operations, hydrodynamics and boundary conditions impact on risk should be a priority as it would greatly improve preparedness to respond in the event of wildfire, and improve the knowledge base needed to make strategic decisions about investment in infrastructure that can reduce the overall vulnerability of the water supply systems to threats from post-fire erosion.

Another key point to note regarding risk mitigation is that the source of the threat is relatively concentrated in a small area of the UY catchment (Figure 6). Therefore, efforts to mitigate risk can be highly targeted. Efforts to reduce sediment loads from debris flow may include channel structures to prevent sediment from entering the reservoir [e.g. check dams: *Abbasi et al.*, 2019] or hillslope treatments that trap hillslope sediment, modify the hydrology, and reduce the probability of a debris flow initiating [*Robichaud et al.*, 2013]. The initiation of debris flows in post-fire settings is highly sensitive to peak runoff [*Kean et al.*, 2011], so any successful attempts to reduce runoff has the potential to substantially reduce the likelihood of a debris flow. There is potential to reduce the probability of large costs if high severity can be limited [*Jones et al.*, 2017]. However, wildfire cannot be eliminated from these ecosystems, and studies indicate that there is not much leverage to reduce the annual area burned by wildfire with fuel reduction methods such as planned fire [*Price et al.*, 2015]. Nonetheless, our analysis indicates that by modifying fire severity, large reduction in risk can be achieved.

Conclusion

Water supply reservoirs in forested catchments are vulnerable to post-fire erosion and sediment transport. However, the risk from such impacts has until now been difficult to quantify because of the lack of suitable models and model integration to represent and link the dominant processes, from rainfall properties, to catchment vulnerability and reservoir propagation of pollutants. In addition, little attention has been given to the development of pragmatic metrics of risk that are relevant and informative for water supply managers and policy makers and enable the cost/benefit of mitigation options to be evaluated easily and transparently. This research has addressed these limitations by coupling reservoir hydrodynamics, post-fire erosion potential, and stochastic rainfall to estimate the probability and duration that turbidity thresholds for treatability are exceeded at the reservoir offtake.

The modelling approach is parsimonious and can be parameterized spatially, focusing the process representation on the dominant controls on the output metric (for example, by representing only debris flow processes). Numerical constraints associated with three dimensional hydrodynamic modelling of a vast number of sediment input realizations (due to the stochastic nature of wildfire and rainfall patterns) have been overcome successfully using a parameter reduction approach to generate a simple relationship between the output metric (probability of days undeliverable) and the input sediment loads from the debris flow process. Lastly, we apply our model to the Upper Yarra catchment that directly delivers water to ~ 4 million residents of Melbourne in SE Australia and show that after high severity wildfire there is a relatively high probability ($0.1 < AEP < 0.3$) of major consequences in the UY reservoir whereby water is untreatable for several months to a year. The duration of this impact is consistent with recent observations of debris flows in other water supply reservoirs in SE Australia.

Acknowledgement

This research was funded by the Australian Research Council (LP150100654), Melbourne Water Corporation, and the Victorian Department of Environment, Land, Water and Planning. All data contributing to the modelling will be made available online at HydroShare: http://www.hydroshare.org/resource/cb639a8d067f4d20810c389918404170

References

Abbasi, N. A., X. Xu, M. E. Lucas-Borja, W. Dang, and B. Liu (2019), The use of check dams in watershed management projects: Examples from around the world, *Science of The Total Environment*, *676,* 683-691. https://doi.org/10.1016/j.scitotenv.2019.04.249

Ball, J., M. Babister, R. Nathan, W. Weeks, E. Weinmann, M. Retallick, and I. Testoni (2016), *Australian rainfall and runoff : a guide to flood estimation*, Commonwealth of Australia, Barton, ACT.

Bladon, K. D., M. B. Emelko, U. Silins, and M. Stone (2014), Wildfire and the Future of Water Supply, *Environmental Science & Technology*, *48*(16), 8936-8943. https://doi.org/10.1021/es500130g

Bowman, D. M., J. K. Balch, P. Artaxo, W. J. Bond, J. M. Carlson, M. A. Cochrane, C. M. et al. (2009), Fire in the Earth system, *Science*, *324*(5926), 481-484. https://doi.org/10.1126/science.1163886

Brown, J. A. H. (1972), Hydrologic effects of a bushfire in a catchment in south-eastern New South Wales, *Journal of Hydrology*, *15*(1), 77-96. https://doi.org/10.1016/0022-1694(72)90077-7

Casulli, V., and R. T. Cheng (1992), Semi-implicit finite difference methods for three-dimensional shallow water flow, *Int. J. Numer. Methods Fluids*, *15*, 629–648. https://doi.org/10.1002/fld.1650150602

Cruz, M. G., A. L. Sullivan, J. S. Gould, N. C. Sims, A. J. Bannister, J. J. Hollis, and R. J. Hurley (2012), Anatomy of a catastrophic wildfire: The Black Saturday Kilmore East fire in Victoria, Australia, *Forest Ecology and Management*, *284*(0), 269-285. http://dx.doi.org/10.1016/j.foreco.2012.02.035

Dallimore, C., and J. Imerger (2006), Upper Yarra Reservoir Thomson Inflow Study, Centre for Water Research report.

Dissanayake, P, H. Hofmann, and F. Peeters (2019), Comparison of results from two 3D hydrodynamic models with field data: internal seiches and horizontal currents, *Inland Waters 9*(2), 239-260. https://doi.org/10.1080/20442041.2019.1580079

Emelko, M. B., U. Silins, K. D. Bladon, and M. Stone (2011), Implications of land disturbance on drinking water treatability in a changing climate: Demonstrating the need for “source water supply and protection” strategies, *Water Research*, *45*(2), 461-472. http://dx.doi.org/10.1016/j.watres.2010.08.051

Emelko, M. B., M. Stone, U. Silins, D. Allin, A. L. Collins, C. H. S. Williams, A. M. Martens, and K. D. Bladon (2016), Sediment-phosphorus dynamics can shift aquatic ecology and cause downstream legacy effects after wildfire in large river systems, *Global Change Biology*, *22*(3), 1168-1184. https://doi.org/10.1111/gcb.13073

Gould, G. K., M. Liu, M. E. Barber, K. A. Cherkauer, P. R. Robichaud, and J. C. Adam (2016), The effects of climate change and extreme wildfire events on runoff erosion over a mountain watershed, *Journal of Hydrology*, *536*, 74-91. http://dx.doi.org/10.1016/j.jhydrol.2016.02.025

Hodges, B., J. Imberger, A. Saggio, and K. B. Winters (2000), Modeling basin-scale internal waves in a stratified lake, *Limnology And Oceanography*, *45*(7), 1603-1620.

Hohner, A. K., C. C. Rhoades, P. Wilkerson, and F. L. Rosario-Ortiz (2019), Wildfires Alter Forest Watersheds and Threaten Drinking Water Quality, *Accounts of Chemical Research*, *52*(5), 1234-1244. https://doi.org/10.1021/acs.accounts.8b00670

Hohner, A. K., K. Cawley, J. Oropeza, R. S. Summers, and F. L. Rosario-Ortiz (2016), Drinking water treatment response following a Colorado wildfire, *Water Research*, *105*, 187-198. https://doi.org/10.1016/j.watres.2016.08.034

Jones, K. W., J. B. Cannon, F. A. Saavedra, S. K. Kampf, R. N. Addington, A. S. Cheng, L. H. MacDonald, C. Wilson, and B. Wolk (2017), Return on investment from fuel treatments to reduce severe wildfire and erosion in a watershed investment program in Colorado, *Journal of Environmental Management*, *198*, 66-77. https://doi.org/10.1016/j.jenvman.2017.05.023

Kean, J. W., D. M. Staley, and S. H. Cannon (2011), In situ measurements of post-fire debris flows in southern California: Comparisons of the timing and magnitude of 24 debris-flow events with rainfall and soil moisture conditions, *Journal of Geophysical Research-Earth Surface*, *116*(F04019). https://doi.org/10.1029/2011jf002005

Key, C. H., and N. C. Benson (2005), Landscape Assessment: Ground measure of severity, the Composite Burn Index; and Remote sensing of severity, the Normalized Burn Ratio, USDA Forest Service, Rocky Mountain Research Station, Ogden, UT.

Khan, S. J., D. Deere, F. D. L. Leusch, A. Humpage, M. Jenkins, and D. Cunliffe (2015), Extreme weather events: Should drinking water quality management systems adapt to changing risk profiles?, *Water Research*, *85*, 124-136. https://doi.org/10.1016/j.watres.2015.08.018

Khan, S. J., D. Deere, F. D. L. Leusch, A. Humpage, M. Jenkins, D. Cunliffe, S. K. Fitzgerald, and B. D. Stanford (2017), Lessons and guidance for the management of safe drinking water during extreme weather events, *Environmental Science: Water Research & Technology*, *3*(2), 262-277. https://doi.org/10.1039/C6EW00165C

Lane, P. N. J., G. J. Sheridan, and P. J. Noske (2006), Changes in sediment loads and discharge from small mountain catchments following wildfire in south eastern Australia, *Journal of Hydrology*(331), 495-510. . https://doi.org/10.1016/j.jhydrol.2006.05.035

Langhans, C., H. G. Smith, D. M. O. Chong, P. Nyman, P. N. J. Lane, and G. J. Sheridan (2016), A model for assessing water quality risk in catchments prone to wildfire, *Journal of Hydrology*, *534*, 407-426. https://doi.org/10.1016/j.geomorph.2017.06.008

Langhans, C., P. Nyman, P. J. Noske, R. E. Van der Sant, P. N. J. Lane, and G. J. Sheridan (2017), Post-fire hillslope debris flows: Evidence of a distinct erosion process, *Geomorphology*, *295*, 55-75. http://dx.doi.org/10.1016/j.jhydrol.2015.12.048

Leak, M., R. Passuello, and B. Tyler (2003), I've seen fire. I've seen rain. I've seen muddy waters that I thought would never clear again., *Waterworks*, *3*, 36-42.

Leonard, B. P., (1991), The ULTIMATE conservative difference scheme applied to unsteady one-dimensional advection. *Computer Methods in Applied Mechanics and Engineering*, *88*, 17–74. https://doi.org/10.1016/0045-7825(91)90232-U

Lyon, J. P., and J. P. O'Connor (2008), Smoke on the water: Can riverine fish populations recover following a catastrophic fire-related sediment slug?, *Austral Ecology*, *33*(6), 794-806. https://doi.org/10.1111/j.1442-9993.2008.01851.x

Madani M., R. Seth, L. F. Leon, R. Valipour, and C. McCrimmon (2020), Three dimensional modelling to assess contributions of major tributaries to fecal microbial pollution of lake St. Clair and Sandpoint Beach, *Journal of Great Lakes Research*, *46*, 159–179. https://doi.org/10.1016/j.jglr.2019.12.005

Marti, C.L., R. Mills, and J Imberger (2011), Pathways of multiple inflows into a stratified reservoir: Thomson Reservoir, Australia, *Advances in Water Resources, 34*(5), 551-561. https://doi.org/10.1016/j.advwatres.2011.01.003

McGuire, L. A., J. W. Kean, D. M. Staley, F. K. Rengers, and T. A. Wasklewicz (2016), Constraining the relative importance of raindrop- and flow-driven sediment transport mechanisms in postwildfire environments and implications for recovery time scales, *Journal of Geophysical Research: Earth Surface*, *121*(11), 2211-2237. https://doi.org/10.1002/2016JF003867

Mills, R, C. Dallimore, C. O’Neill, K. Cinque, and S. Haydon (2011). Development and use of a decision support tool for supporting the operation of Melbourne Water’s drinking water reservoirs, Victoria, Australia, *19th International Congress on Modelling and Simulation,* 12–16 December 2011, Perth, Australia.

Moody, J. A., B. A. Ebel, P. Nyman, D. A. Martin, C. R. Stoof, and R. McKinley (2015), Relations between soil hydraulic properties and burn severity, *International Journal of Wildland Fire*, *25*(3), 279-293. http://dx.doi.org/10.1071/WF14062

Morillo, S., J. Imberger, and J. Antenucci (2006), Modifying the residence time and dilution capacity of a reservoir by altering internal flow-paths, *Intl. J. River Basin Manage.*, *4(4)*, 255-271. https://doi.org/10.1080/15715124.2006.9635295

Murphy, S. F., J. H. Writer, R. B. McCleskey, and D. A. Martin (2015), The role of precipitation type, intensity, and spatial distribution in source water quality after wildfire, *Environ Res Lett*, *10*(8), 084007. https://doi.org/10.1088/1748-9326/10/8/084007

Noske, P. J., P. Nyman, P. N. J. Lane, and G. J. Sheridan (2016), Effects of aridity in controlling the magnitude of runoff and erosion after wildfire, *Water Resources Research*, *52*(6). https://doi.org/4338-4357. 10.1002/2015wr017611

Nunes, J., S. Doerr, G. Sheridan, J. Neris, C. Santín, M. Emelko, U. Silins, P. Robichaud, W. Elliot, and J. Keizer (2018), Assessing water contamination risk from vegetation fires: Challenges, opportunities and a framework for progress, *Hydrological Processes*, *32*(5), 687-694. https://doi.org/10.1002/hyp.11434

Nyman, P., G. J. Sheridan, and P. N. Lane (2013), Hydro-geomorphic response models for burned areas and their applications in land management, *Progress in Physical Geography*, *37*(6), 787-812. https://doi.org/10.1177/0309133313508802

Nyman, P., G. J. Sheridan, H. G. Smith, and P. N. J. Lane (2011), Evidence of debris flow occurrence after wildfire in upland catchments of south-east Australia, *Geomorphology*, *125*(3), 383-401. https://doi.org/10.1016/j.geomorph.2010.10.016

Nyman, P., H. G. Smith, C. B. Sherwin, C. Langhans, P. N. J. Lane, and G. J. Sheridan (2015), Predicting sediment delivery from debris flows after wildfire, *Geomorphology*, *250*, 173-186. http://dx.doi.org/10.1016/j.geomorph.2015.08.023

Nyman, P., W. A. C. Box, J. C. Stout, G. J. Sheridan, S. D. Keesstra, P. N. J. Lane, and C. Langhans (2020), Debris-flow-dominated sediment transport through a channel network after wildfire, *Earth Surface Processes and Landforms*, *45*(5), 1155-1167. https://doi.org/10.1002/esp.4785

Ollerenshaw, A., P. Dahlhaus, K. McDonald, J. Courvisanos, M. Graymore, H. Thompson, H. Sheil, A. Miner, and J. Corbett (2014), Understanding the 2011 Grampians Natural Disaster, addressing the risk and resilience, 1-121 pp, Centre for eCommerce and Communications, Federation University Australia, Ballarat.

Paschalis, A., P. Molnar, S. Fatichi, and P. Burlando (2013), A stochastic model for high-resolution space-time precipitation simulation, *Water Resources Research*, *49*(12), 8400-8417. https://doi.org/10.1002/2013WR014437

Peleg, N., Fatichi, S., Paschalis, A., Molnar, P., and Burlando, P. (2017), An advanced stochastic weather generator for simulating 2-D high-resolution climate variables, *J. Adv. Model. Earth Syst.*, 9, 1595– 1627. https://doi.org/10.1002/2016MS000854

Peleg, N., Molnar, P., Burlando, P., and Fatichi, S.: Exploring stochastic climate uncertainty in space and time using a gridded hourly weather generator, *Journal of Hydrology*, 571, 627-641. https://doi.org/10.1016/j.jhydrol.2019.02.010

Porter, J. H., Matonse, A.H., Frei, A. (2015): The New York City Operations Support Tool (OST): Managing Water for Millions of People in an Era of Changing Climate and Extreme Hydrological Events, *Journal of Extreme Events* 02(02), 1550008. https://doi.org/10.1142/S2345737615500086

Price, O. F., T. D. Penman, R. A. Bradstock, M. M. Boer, and H. Clarke (2015), Biogeographical variation in the potential effectiveness of prescribed fire in south-eastern Australia, *Journal of Biogeography*, *42*(11), 2234-2245. https://doi.org/10.1111/jbi.12579

Productivity Commission (2011), Australia's urban water sector. , in *Inquiry report*, edited, pp. 1-332, Commonwealth Government of Australia, Canberra.

Rhoades, C. C., D. Entwistle, and D. Butler (2011), The influence of wildfire extent and severity on streamwater chemistry, sediment and temperature following the Hayman Fire, ColoradoA, *International Journal of Wildland Fire*, *20*(3), 430-442. https://doi.org/10.1071/WF09086

Robichaud, P. R., W. J. Elliot, S. A. Lewis, and M. E. Miller (2016), Validation of a probabilistic post-fire erosion model, *International Journal of Wildland Fire*, *25*(3), 337-350. https://doi.org/10.1071/WF14171

Robichaud, P. R., J. W. Wagenbrenner, S. A. Lewis, L. E. Ashmun, R. E. Brown, and P. M. Wohlgemuth (2013), Post-fire mulching for runoff and erosion mitigation Part II: Effectiveness in reducing runoff and sediment yields from small catchments, *CATENA*, *105*, 93-111. https://doi.org/10.1016/j.catena.2012.11.016

Ryu, I., S. Yu, and S. Chung (2020), Characterizing Density Flow Regimes of Three Rivers with Different Physicochemical Properties in a Run-Of-The-River Reservoir, *Water*, *12*(3), 717. https://doi.org/10.3390/w12030717

Sankey, J. B., J. Kreitler, T. J. Hawbaker, J. L. McVay, M. E. Miller, E. R. Mueller, N. M. Vaillant, S. E. Lowe, and T. T. Sankey (2017), Climate, wildfire, and erosion ensemble foretells more sediment in western USA watersheds, *Geophysical Research Letters*, *44*(17), 8884-8892. https://doi.org/10.1002/2017GL073979

Smith, H. G., G. J. Sheridan, P. N. J. Lane, P. Nyman, and S. Haydon (2011), Wildfire effects on water quality in forest catchments: A review with implications for water supply, *Journal of Hydrology*, *396*(1-2), 170-192. https://doi.org/10.1016/j.jhydrol.2010.10.043

Stevens, M. R., S. Haydon, K. Cinque, and P. Yeates (2012), Modelling storages of an unfiltered supply, paper presented at Water Quality Technology Conference and Exposition American Water Works Association, Toronto, Canada, 4-8 November.

Stone, M., M. B. Emelko, I. G. Droppo, and U. Silins (2011), Biostabilization and erodibility of cohesive sediment deposits in wildfire-affected streams, *Water Research*, *45*(2), 521-534. https://doi.org/10.1016/j.watres.2010.09.016

Thompson, M. P., and D. E. Calkin (2011), Uncertainty and risk in wildland fire management: a review, *Journal of Environmental Management*, *92*(8), 1895-1909. https://doi.org/10.1016/j.jenvman.2011.03.015

Tranmer, A.W., C. L. Marti, D. Tonina, R. Benjankar, D. Weigel, L. Vilhena et al. (2018), A hierarchical modelling framework for assessing physical and biochemical characteristics of a regulated river, *Ecological Modelling*, *368*, 78-93. https://doi.org/10.1016/j.ecolmodel.2017.11.010

Trolle, D., D.P. Hamilton, M.R. Hipsey, K. Bolding, J. Bruggeman, W.M. Mooij, et al. (2012), A community-based framework for aquatic ecosystem models, *Hydrobiologia*, *683*(1), 25-34. https://doi.org/10.1007/s10750-011-0957-0

Valerio, G., M. Pilotti, M. P. Lau, and M. Hupfer (2019), Oxycline oscillations induced by internal waves in deep Lake Iseo, *Hydrol. Earth Syst. Sci.*, *23*, 1763–1777. https://doi.org/10.5194/hess-23-1763-2019

Valipour R., Y. R. Rao, L. F. León, and D. Depew (2019), Nearshore-offshore exchanges in multi-basin coastal waters: Observations and three-dimensional modeling in Lake Erie, *Journal f Great Lakes Research*, *45*, 50–60. https://doi.org/10.1016/j.jglr.2018.10.005

Van der Sant, R. E., P. Nyman, P. J. Noske, C. Langhans, P. N. J. Lane, and G. J. Sheridan (2018), Quantifying relations between surface runoff and aridity after wildfire, *Earth Surface Processes and Landforms*, *43*(10), 2033-2044. https://doi.org/10.1002/esp.4370

Vieira, D. C. S., S. A. Prats, J. P. Nunes, R. A. Shakesby, C. O. A. Coelho, and J. J. Keizer (2014), Modelling runoff and erosion, and their mitigation, in burned Portuguese forest using the revised Morgan–Morgan–Finney model, *Forest Ecology and Management*, *314*, 150-165. https://doi.org/10.1016/j.foreco.2013.12.006

White, I., A. Wade, M. Worthy, N. Mueller, T. Daniell, and R. Wasson (2006), The vulnerability of water supply catchments to bushfires: Impacts of the January 2003 wildfires on the Australian Capital Territory, *Australian journal of water resources 10*(2), 1-16. https://doi.org/10.1080/13241583.2006.11465291

Woolhiser, D. A., R. E. Smith, and D. C. Goodrich (1990), *KINEROS, A Kinematic Runoff and Erosion Model: Documentation and User Manual*.

Writer, J. H., A. Hohner, J. Oropeza, A. Schmidt, K. M. Cawley, and F. L. Rosario-Ortiz (2014), Water treatment implications after the High Park Wildfire, Colorado, *Journal: American Water Works Association*, *106*(4), E189-E199. https://doi.org/10.5942/jawwa.2014.106.0055

Zamani, B., and M. Koch (2020), Comparison Between Two Hydrodynamic Models in Simulating Physical Processes of a Reservoir with Complex Morphology: Maroon Reservoir, *Water*, *12*(3), 814. https://doi.org/10.3390/w12030814

Figures

Figure 1. a) Model framework showing the workflow for producing a risk metric from transfer functions that couple an erosion model with a reservoir hydrodynamics model. b) Example of the final risk metrics which is the probability of consequence.

Figure 2. Map showing regional context and the Upper Yarra (UY) catchment. a) A digital terrain model (20m) of eastern upland of Victoria with i) location of post-fire debris flows used in developing a model of debris flow magnitude, ii) the location of experiment sites used to evaluate the surface runoff model and, iii) wildfires in 2007 and 2009 that were used in calibration and testing the erosion model (see Supporting Information). Wildfires from 2009 (difference Normalized Burn Ratio, or dNBR, shown in map) were used in developing wildfire scenarios in the UY catchment, where the model is implemented. The dNBR was calculated from Landsat imagery using methods described in *Key and Benson* [2005] and scaled by a factor of 10^3. b) The distribution of forest types in the UY catchment and the 4 locations (Site 1-4) where sediment input was simulated in the hydrodynamic model.

Figure 3. Fire severity distributions for zero-order headwaters in the Kilmore-Murrundindi (KM) fire. High and low fire severity distributions are obtained for areas that burned before and after 10pm on the day that the fire started (see Figure 2a). High and low severities generally correspond to crown and understory fires, respectively.

Figure 4. The concentration of total suspended clay at the dam wall offtake for low and high clay inputs (M_c) at sites 1-4. a, b) Site 1, c-d) Site 2, d-e) Site 3 and e-f) Site 4. The thick line illustrates total suspended clay (grain size ≤ 0.002 mm), with each gray line indicating contribution from size fractions 0.001 - 0.002 mm. Dashed line horizontal line is the upper limit (10 mg L^{-1}) of the treatability threshold.

Figure 5. Relations between the number of days that suspended sediment concentrations exceed water quality thresholds at the water offtake given different sediment loads input at sites 1-4 for suspended sediment concentration thresholds of 5 - 10 mg L^{-1} (which correspond to ~ 5 NTU).

Figure 6. Distributions of debris flow rainfall thresholds (I_{12}) and annual exceedance probabilities (AEP) in headwaters for high fire severity (a, b) and low fire severity (c, d). Values are the median of 10 samples of fire severity from the distributions in Figure 3.

Figure 7. Scenarios of clay delivery (M_c) to the Upper Yarra reservoir and disruptions to treatability as a result of post-fire debris flows for high severity wildfire (a,b) and low severity wildfire (c,d). Annual exceedance probabilities (AEP) for M_c are obtained using design storms with depth area reduction factor and rain fields from Space-Time Realizations for Areal Precipitation (STREAP). For both rainfall types, the outcome from storms with the same AEP are variable depending on spatial distribution of peak intensities. All distributions are equally likely. The conversion from M_c to days of untreatable water stems from equation 1 where $D_{>th} = 0.51{M_c}^{0.77} - 44$ (Figure 5), and assumes a treatability threshold between 5 and 10 mg L^{-1} (~5 NTU). Results in the shaded region of c) and d) fall outside the range of sediment input scenarios used in the hydrodynamic simulations (Figure 5).

Tables

Table 1. Change in the simulated number of days the water is undeliverable water at Site 1 between events in summer and autumn.

Site 1	Limit value	Summer	Autumn	Change
Lowest	5 mg/l	7 d	0 d	-
Highest	5 mg/l	231 d	303 d	+31%
	7 mg/l	170 d	257 d	+51%
	10 mg/l	107 d	152 d	+42%

Table 2. Annual exceedance probabilities (AEP) for durations of water supply interruptions ($D_{>th}$) for simulations using two different methods of generating rainstorms.

Days exceeding threshold ($D_{>th}$)	Mass of clay delivery	AEP design storm	AEP STREAP
days	[Mg]	[-]	[-]
	Low severity fire		
50	876	0.19	0.15
100	1525	0.15	0.09
300	4721	0.06	<0.01
	High severity fire		
50	876	0.45	0.39
100	1525	0.42	0.28
300	4721	0.29	0.10

Table 3. The contribution of different model components to error in predictions.

Components	Method	StdDev	CV [%]	Uncertainty in $D_{>th}$ [days][4]		
				$D_{>th}$ = 1 month	$D_{>th}$ = 6 months	$D_{>th}$ = 12 months
DF threshold	Range[1]	1.13	3.7	±3.7	±11	±20
($28.3 \leq b \leq 32.2$)				(12)	(6.2)	(5.6)
Load [Mg]	RMSE[2]	112	13	±3.5	±20	±41
(obs vs pred)				(12)	(11)	(11)
Clay content [%]	From sample	0.025	3.1	±0.8	±4.9	±9.9
(sample distribution)				(2.7)	(2.7)	(2.7)
Input location and turbidity	RMSE[3]	52	29	±52	±52	±52
threshold				(173)	(28)	(14)
Season	Range[1]	19.1	11	±3.3	±20	±41
(autumn or summer)				(11)	(11)	(11)

[1]Assuming uniform distributions where stdev=(max-min)/sqrt(12) (see Supporting Informationfor description of parameter *b*).

[2]From data in Nyman et al 2013 (see Supporting Information).

[3]From fitted function (Eqn. 1) in Figure 5

[4]Values in () are the error in units of %

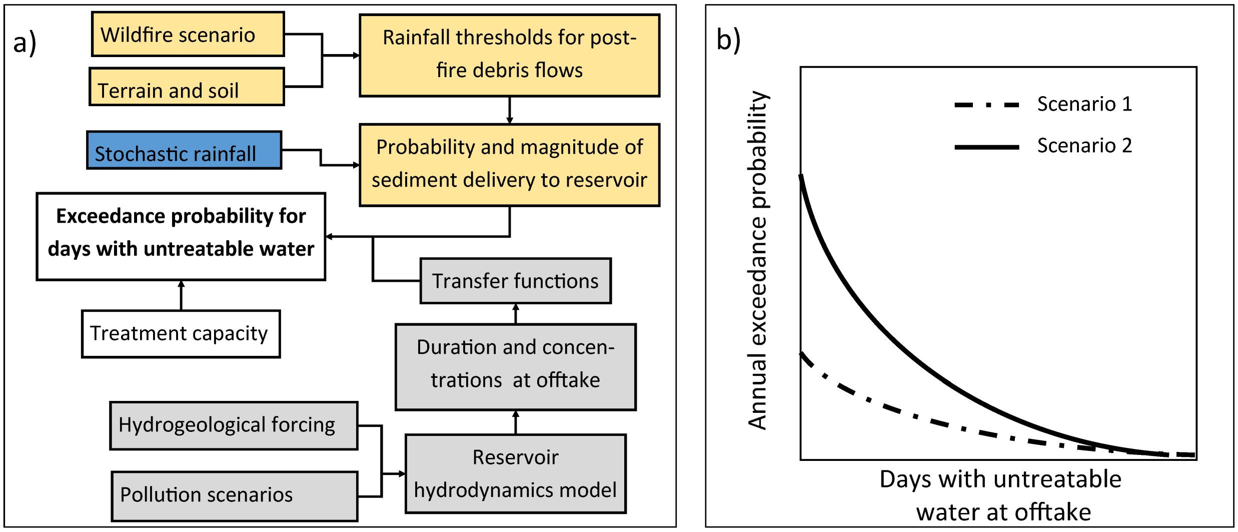
a)
Wildfire scenario
Terrain and soil
Rainfall thresholds for post-fire debris flows
Stochastic rainfall
Probability and magnitude of sediment delivery to reservoir
Exceedance probability for days with untreatable water
Transfer functions
Treatment capacity
Duration and concentrations at offtake
Hydrogeological forcing
Pollution scenarios
Reservoir hydrodynamics model
b)
Scenario 1
Scenario 2
Annual exceedance probability
Days with untreatable water at offtake

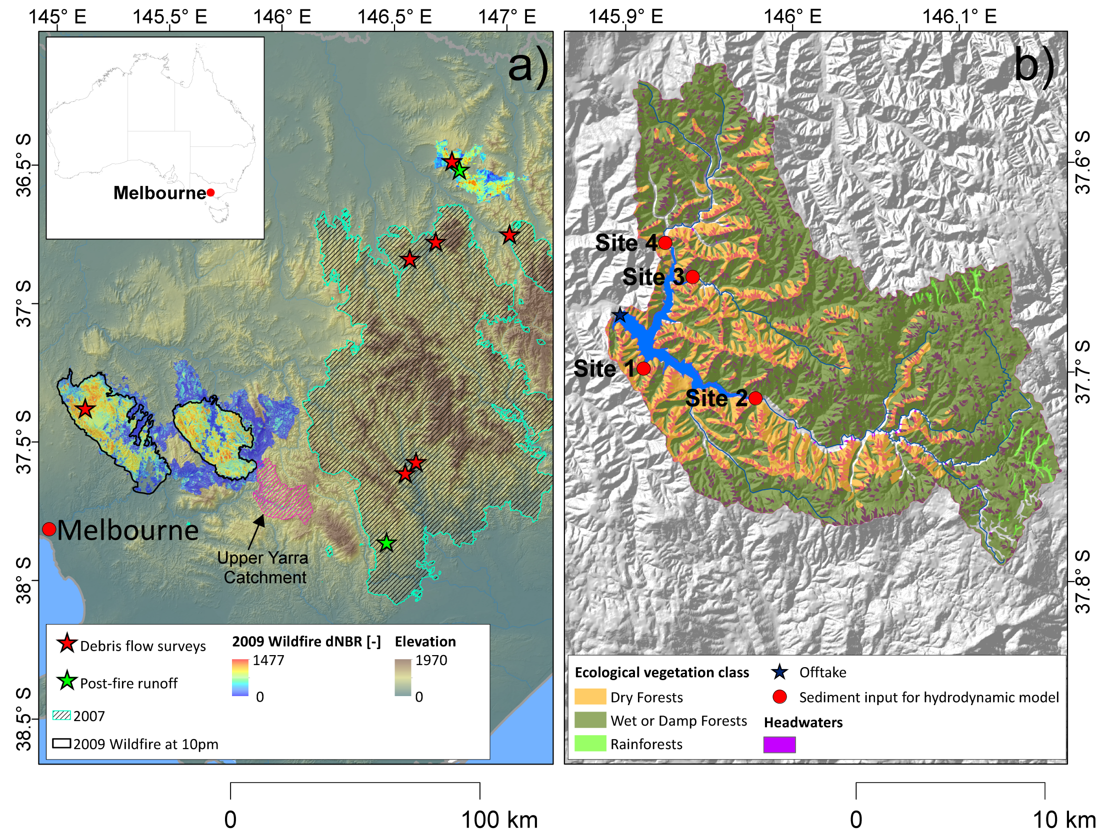
145° E
145.5° E
146° E
146.5° E
147° E
36.5° S
37° S
37.5° S
38° S
38.5° S
a)
Melbourne
Melbourne
Upper Yarra Catchment
Debris flow surveys
Post-fire runoff
2007
2009 Wildfire at 10pm
2009 Wildfire dNBR [-]
1477
0
Elevation
1970
0
0
100 km
145.9° E
146° E
146.1° E
37.6° S
37.7° S
37.8° S
b)
Site 4
Site 3
Site 1
Site 2
Ecological vegetation class
Dry Forests
Wet or Damp Forests
Rainforests
Offtake
Sediment input for hydrodynamic model
Headwaters
0
10 km

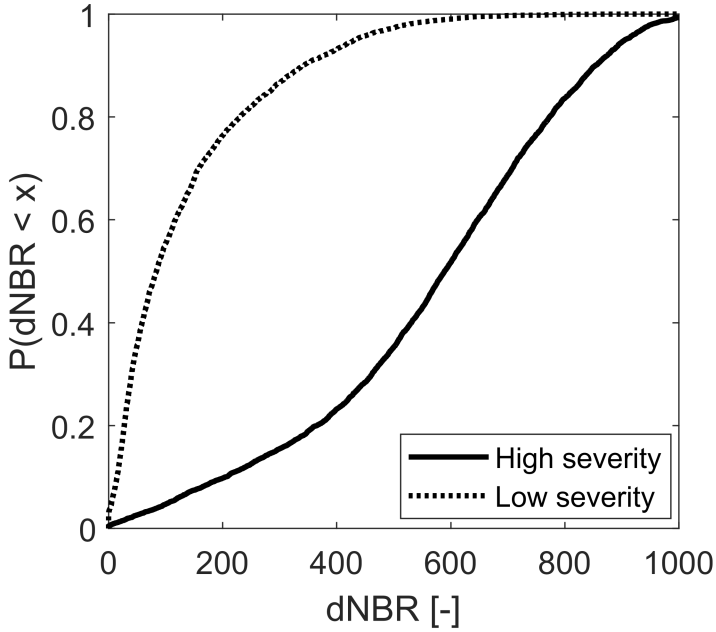

1
0.8
0.6
0.4
0.2
0
P(dNBR < x)
0
200
400
600
800
1000
dNBR [-]
High severity
Low severity

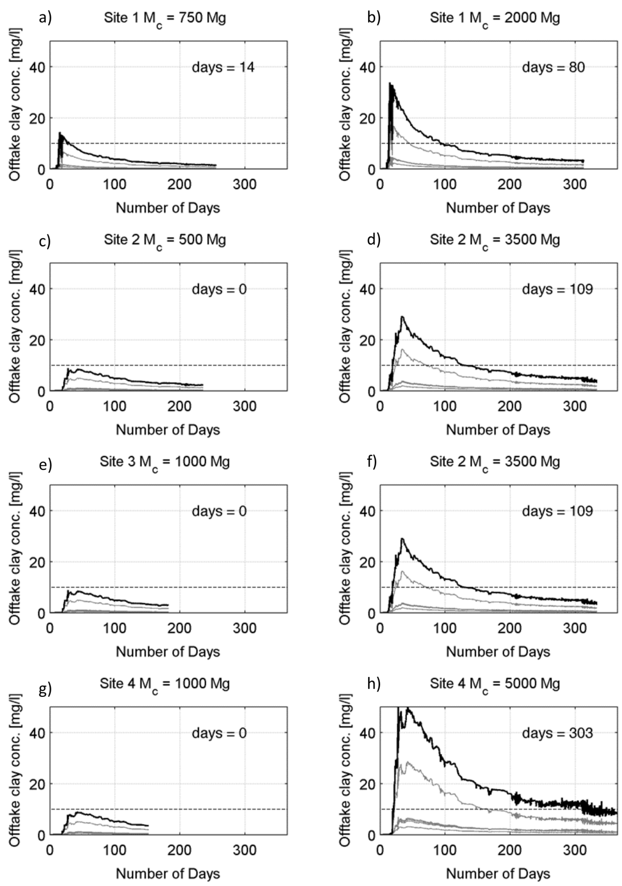
a)
Site 1 M_c = 750 Mg
days = 14
b)
Site 1 M_c = 2000 Mg
days = 80
c)
Site 2 M_c = 500 Mg
days = 0
d)
Site 2 M_c = 3500 Mg
days = 109
e)
Site 3 M_c = 1000 Mg
days = 0
f)
Site 2 M_c = 3500 Mg
days = 109
g)
Site 4 M_c = 1000 Mg
days = 0
h)
Site 4 M_c = 5000 Mg
days = 303
Offtake clay conc. [mg/l]
Number of Days
0
20
40
0
100
200
300

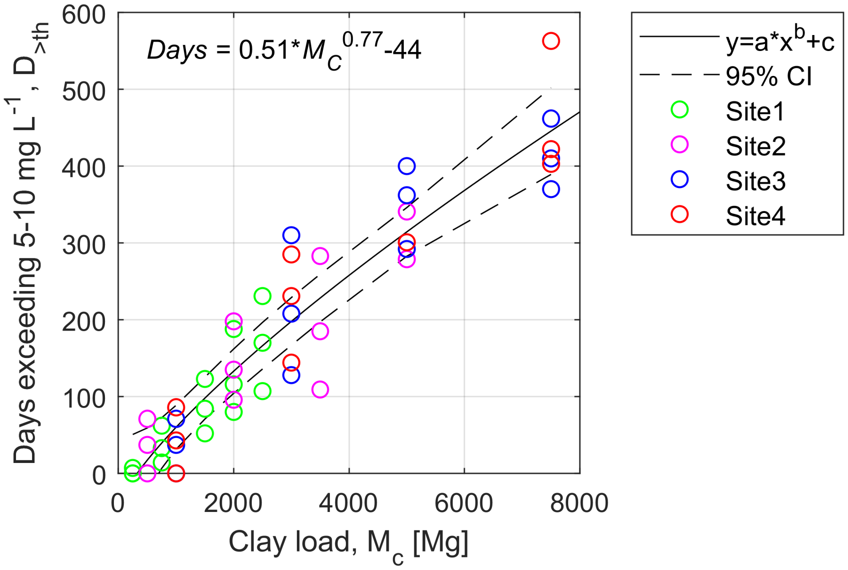

Days = 0.51*M_C^0.77-44
Days exceeding 5-10 mg L^-1, D_>th
Clay load, M_c [Mg]
0
100
200
300
400
500
600
0
2000
4000
6000
8000
y=a*x^b+c
95% CI
Site1
Site2
Site3
Site4

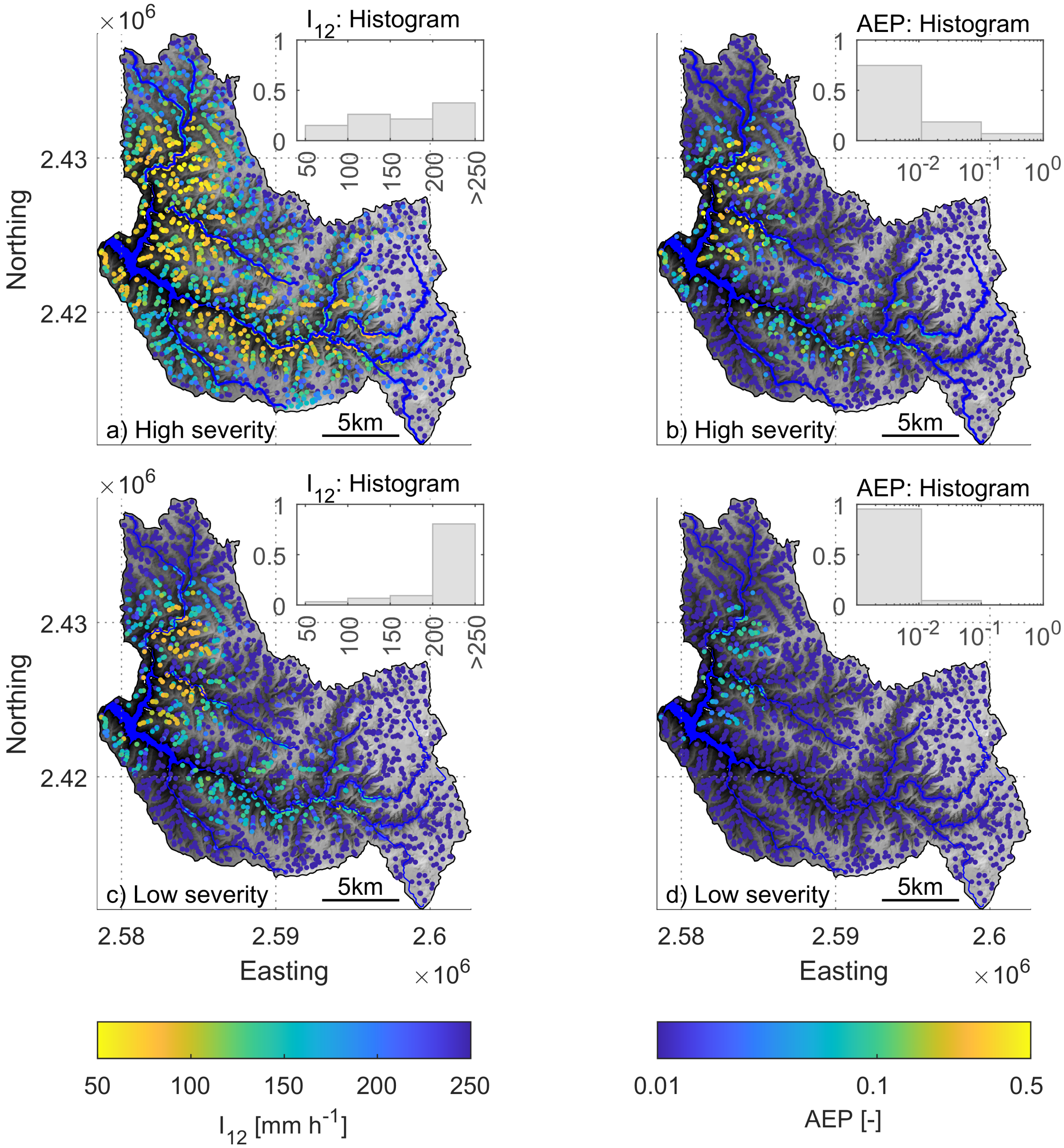

×10^6
I12: Histogram
AEP: Histogram
1
0.5
0
50
100
150
200
>250
10^-2
10^-1
10^0
2.43
2.42
Northing
a) High severity
b) High severity
c) Low severity
d) Low severity
5km
2.58
2.59
2.6
Easting
×10^6
50
100
150
200
250
I12 [mm h^-1]
0.01
0.1
0.5
AEP [-]

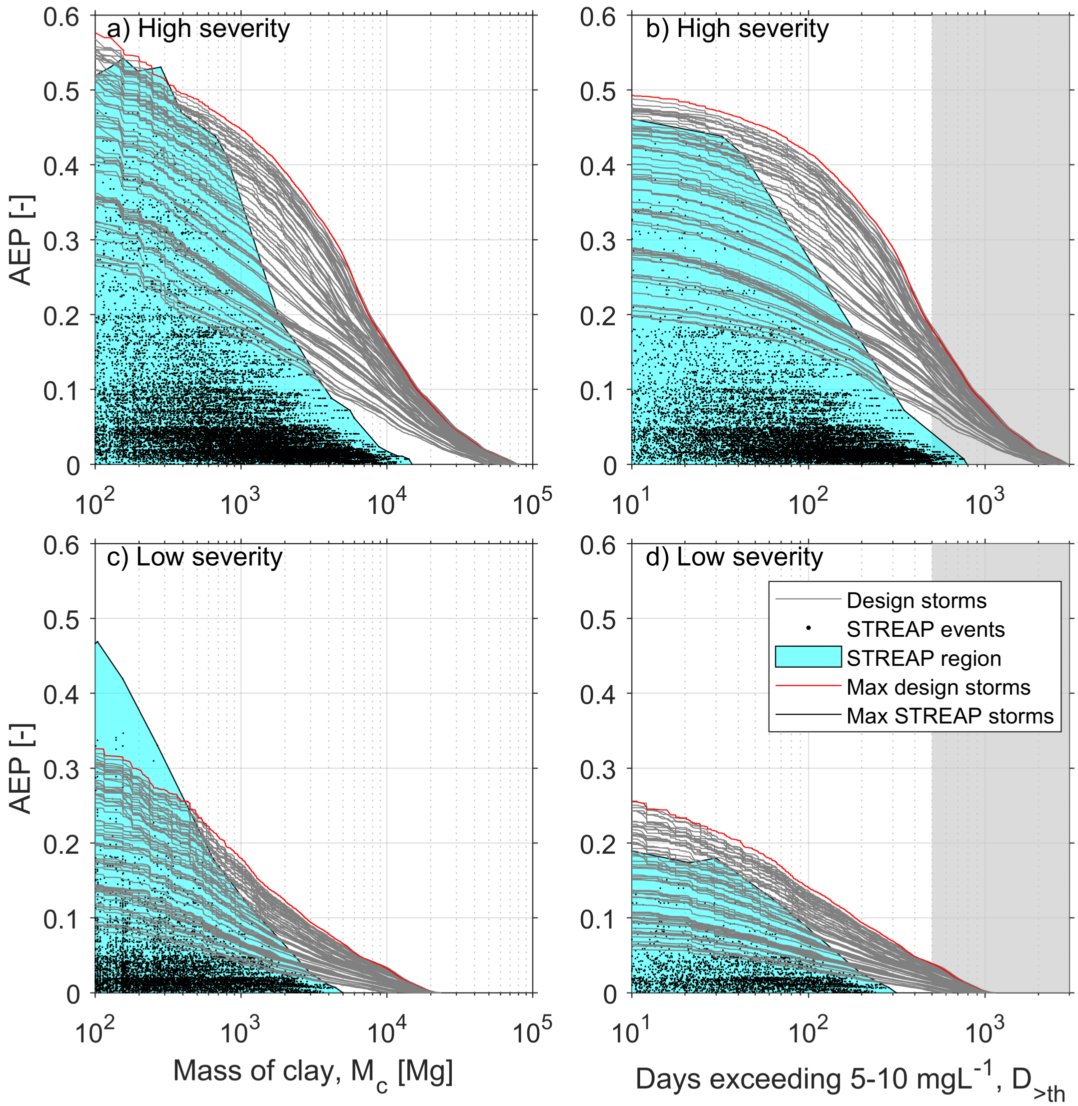
a) High severity
b) High severity
c) Low severity
d) Low severity
AEP [-]
Mass of clay, M_c [Mg]
Days exceeding 5-10 mgL^-1, D_>th
Design storms
STREAP events
STREAP region
Max design storms
Max STREAP storms